POLITECNICO DI TORINO
Repository ISTITUZIONALE

Strong and weak form solutions of curved beams via Carrera's unified formulation

(Article begins on next page)

25 April 2024

Strong and weak form solutions of curved beams via Carrera's Unified Formulation

G. De Pietro[*],
Luxembourg Institute of Science and Technology,
5, avenue des Hauts-Fourneaux, L-4362 Esch-sur-Alzette, Luxembourg and
Politecnico di Torino, c.so Duca degli Abruzzi 24, 10129 Turin, Italy

A. G. de Miguel[†], E. Carrera[‡]
Politecnico di Torino,
c.so Duca degli Abruzzi 24, 10129 Turin, Italy

G. Giunta[§], S. Belouettar[¶],
Luxembourg Institute of Science and Technology,
5, avenue des Hauts-Fourneaux, L-4362 Esch-sur-Alzette, Luxembourg

A. Pagani[‖]
Politecnico di Torino,
c.so Duca degli Abruzzi 24, 10129 Turin, Italy

Author for correspondence:
Gabriele De Pietro, Ph.D. student,
Materials Research and Technology Department,
Luxembourg Institute of Science and Technology,
5, avenue des Hauts-Fourneaux,
L-4362 Esch-sur-Alzette, Luxembourg.
tel: +352 275 888 1,
fax: +352 275 885,
e-mail: gabriele.depietro@list.lu

---

[*]Ph.D. student.
[†]Ph.D. student.
[‡]Full Professor.
[§]Research scientist.
[¶]Research scientist.
[‖]Research scientist.

Abstract

In this paper, the mechanical behaviour of three-dimensional curved beams is investigated through closed-form solution as well as one-dimensional finite elements based on Carrera's Unified Formulation (CUF). CUF is a hierarchical formulation in which the approximation order of the displacement field is a free parameter of the analysis. Therefore, refined models accounting for higher-order effects such as shear deformation and local warping can be obtained with no need for ad hoc formulations. The Principle of Virtual Displacements (PVD) is used in order to derive both strong and weak formulations. For the latter, locking phenomena typical of curved finite elements are tackled by means of a Mixed Interpolation of Tensorial Components (MITC). Numerical results for different boundary conditions and loading configurations are investigated and validated towards elasticity solutions and commercial software finite elements showing that the proposed formulation can lead to an accurate evaluation of the displacement and stress fields with reduced computational costs.

1 Introduction

Curved beam elements find applications in many mechanical, civil and aerospace engineering systems, such as turbine blades, stiffeners, arch bridges and long-span roof structures. Curved structural components are often analysed by employing straight finite elements together with a very refined mesh in order to minimize the geometrical error. A more accurate and efficient model can be obtained by developing theories that account for the curvature of the beam axis. On the other hand, curved beams are more complex to handle due to the coupling between the axial and bending deformations and, in the framework of finite elements, the presence of locking phenomena which can negatively influence the accuracy of the results. Extensive research has been carried out in the past in this area in order to develop accurate curved beam models. A brief overview of the existing literature about analytical solutions and finite elements formulation for the static mechanical analysis of curved beams is reported below.

Elasticity solutions of common case studies for curved beam structures can be found in Timoshenko and Goodier [1]. Analytical expressions based on Volterra integral for the shear and radial stresses were provided by Yu and Nie [2]. Tufekci and Arpaci [3] provided analytical solutions for axial- and shear-flexible planar curved beams with variable cross-section by the initial value method. Gimena et al. [4] provided analytical solutions for three-dimensional circular arches and balcony structures. The formulation of the curved beam was derived in global Cartesian coordinates and a twelve lower-triangular governing differential equations system was solved through successive integrations.

As far as finite element analysis is concerned, attention was concentrated on the performance evaluation of the element. Higher-order shape functions were proven to yield significantly more accurate results at the expense of computation efficiency. Most common techniques that have been used in order to alleviate locking phenomena include the strain element technique, the selective or reduced integration and the use of modified isoparametric elements. Babu and Prathap [5] derived a locking-free thick curved beam finite element in which a linear interpolation for displacements and rotation was assumed. Axial and shear strain fields were indirectly derived from the displacements through strain smoothing in order to improve the efficiency of the element. Tabarrok et al. [6] proposed a finite element model for spatially curved rods by assuming constant strain and using displacement modes as basis functions for the formulation of the elemental matrices. Reddy and Volpi [7] carried out a mixed finite element investigation for the analysis of circular arches. Governing equations were obtained by Timoshenko-Mindlin-Reissner's assumptions. The equivalence between mixed problem and standard problem with selective reduced integration was demonstrated. Choi and Lim [8] formulated general curved beam elements on the basis of Timoshenko's beam theory. A two-node element with constant strain field and a three-node element with linear strain field assumption were proposed for the displacements and stress resultants prediction in rings and curved cantilever beams. A three-node locking-free curved beam element was proposed by Lee and Sin [9], in which the nodal unknowns were curvatures instead of pure displacements.

Litewka and Rakowski [10] formulated a two-node locking-free curved beam finite element including the effects of flexural, axial and shear deformations. Exact trigonometric shape functions for the case of constant curvature were employed in order to derive the element stiffness matrix. Raveendranath et al. [11] presented a three-node curved element based on Timoshenko's beam theory for static and free-vibration analyses of several curved structures. A quartic-order polynomial for the flexural rotation was a-priori assumed and a novel way of deriving the polynomial interpolations for the displacements was presented, by employing the force-moment and moment-shear equilibrium equations. A novel geometrically exact finite-strain beam theory was proposed by Zupan and Saje [12]. A modified version of the principle of the virtual work was proposed, where the strain vectors were the only functions that needed to be interpolated. The strain field was assumed to be linear and a collocation algorithm was used in order to solve the governing equations. Zhu and Meguid [13] proposed a three-node element based on Euler-Bernoulli's beam theory. Coupled consistent polynomial displacement fields satisfying the membrane locking-free requirement were employed. Quintic transverse displacement interpolation functions were used to represent the bending deformation of the beam, while the assumption of linear variation was considered for the membrane and torsional shear strain fields. In-plane arch structures were studied by Nascimbene [14] by three-node and five-node shear-flexible curved beam elements based on Mindlin-Reissner's theory. Locking issues were tackled by an appropriate choice of the shear and membrane strain functions. Tang et al. [15] presented a two-node displacement-based curved beam element in which the interpolation function for the displacements is based on the infinitesimal straight beam section in order to avoid the coupling between tangential and radial displacement in the strain field. Zhang et al. [16] presented an isogeometric approach for the formulation of three-dimensional curved beams. Non-uniform rational b-spline interpolation was used for both geometry and finite element unknowns. Locking phenomena were tackled by increasing the order of the interpolation. Most of the existing studies on curved beam elements assume classical kinematic hypotheses, such as Euler-Bernoulli's and Timoshenko's theory. These solutions can be adequate for a number of common structural analyses involving very slender components. Nevertheless, in the case of thicker beams, they lead to inaccuracies in the displacement and stress field prediction due to higher-order shear deformation effects and local cross-sectional warping.

In this paper, a mechanical analysis of slender and thick curved beam structures is carried out via a closed-form Navier-type analytical solution as well as a weak form finite element solution based on CUF. In the framework of CUF, advanced one-dimensional elements can be formulated via a compact notation of the displacement field expansion over the cross-section. The approximation order of the displacement field is a free input of the structural analysis. Therefore, by appropriately choosing the order, shear and torsional deformation as well as cross-section in- and out-of-plane warping can be straightforwardly and implicitly accounted for with no need for ad hoc formulations. CUF also allows deriving finite elements with a generic number of nodes. Cubic C^0 elements are used in the following numerical investigations,

unless stated otherwise. CUF had been previously proposed for plate and shell structures, see Carrera [17] and Biscani et al. [18] and it has been lately extended to beams, see Carrera et al. [19] and Carrera and Giunta [20]. 1D CUF theories based on Taylor expansion as well as Legendre expansion of the displacement field are adopted in this work. This formulation has been thoroughly investigated in the framework of straight beams for isotropic as well as laminated composite structures by Giunta et al. [21, 22], Carrera et al. [23, 24] and Pagani et al. [25]. Locking phenomena are avoided via MITC, which was initially proposed for beam elements by Bathe [26] and recently extended to higher-order beam models by Carrera et al. [27]. Numerical investigations are carried out for different boundary conditions, external loadings and slenderness ratios of the beam. Displacement and stress field over the beam domain are compared with available literature results, elasticity solutions and commercial 2D and 3D finite element solutions showing that a computationally efficient prediction of the mechanical response of curved beams can be obtained via the proposed formulation.

2 Geometrical and Constitutive Relations

2.1 Geometry of a curved beam

A curved beam is a solid generated by the translation of a plane cross-section along a generic curved axis. Let $\mathbf{r}(s)$ be the vector defining the beam axis in $\mathbb{R}^3$ and s the independent variable corresponding to the length of the arc. The Frenet-Seret coordinate system associated to a unit-speed curve is defined by an orthonormal vector basis $\{\boldsymbol{t},\boldsymbol{b},\boldsymbol{n}\}$, being:

$$\mathbf{t}(s) = \frac{d\mathbf{r}(s)}{ds} \qquad \mathbf{n}(s) = \frac{\frac{d^2\mathbf{r}(s)}{ds^2}}{\left\|\frac{d^2\mathbf{r}(s)}{ds^2}\right\|} \qquad \mathbf{b}(s) = \mathbf{t}(s) \times \mathbf{n}(s) \tag{1}$$

where $\boldsymbol{t}$ is the tangent versor to the curve at each s location, whereas $\boldsymbol{n}$ and $\boldsymbol{b}$ are the principal normal and bi-normal unit vector, respectively. Figure 1 shows the Frenet-Seret frame embedded in a curved beam. The derivatives of the $\{\boldsymbol{t},\,\boldsymbol{n},\,\boldsymbol{b}\}$ triad are provided by the Ferret-Seret formulae, which can be written in a matrix form as:

$$\frac{d}{ds} \left\{ \begin{array}{c} \mathbf{t} \\ \mathbf{n} \\ \mathbf{b} \end{array} \right\} = \left[\begin{array}{ccc} 0 & \kappa & 0 \\ -\kappa & 0 & \tau \\ 0 & -\tau & 0 \end{array} \right] \left\{ \begin{array}{c} \mathbf{t} \\ \mathbf{n} \\ \mathbf{b} \end{array} \right\} \tag{2}$$

where κ and τ are the curvature and torsion, respectively, of the beam axis and they are defined as:

$$\kappa(s) = \left\|\frac{d^2\mathbf{r}(s)}{ds^2}\right\| \qquad \tau(s) = -\mathbf{n}(s) \cdot \frac{d\mathbf{b}(s)}{ds} \tag{3}$$

The curvature measures the deviation of the curve from being a straight line, whereas the geometric torsion is the amount by which the curve does not lie in a plane. The reference system $\{\mathbf{e_1},\,\mathbf{e_2},\,\mathbf{e_3}\}$, with $\mathbf{e_1} \equiv \mathbf{t}$ and $\mathbf{e_2},\,\mathbf{e_3}$ being the unit vectors aligned to the principal axes of the beam cross-section could also be introduced. In the most general case, $\mathbf{e_2}$ and

$\mathbf{e_3}$ are rotated by an angle θ with respect to the principal normal and binormal unit vectors, therefore:

$$\left\{ \begin{array}{c} \mathbf{e_1} \\ \mathbf{e_2} \\ \mathbf{e_3} \end{array} \right\} = \left[\begin{array}{ccc} 1 & 0 & 0 \\ 0 & \cos\theta & \sin\theta \\ 0 & -\sin\theta & \cos\theta \end{array} \right] \left\{ \begin{array}{c} \mathbf{t} \\ \mathbf{n} \\ \mathbf{b} \end{array} \right\} \tag{4}$$

From Eq. (2) and (4), the following differential equations can be obtained:

$$\frac{d}{ds} \left\{ \begin{array}{c} \mathbf{e_1} \\ \mathbf{e_2} \\ \mathbf{e_3} \end{array} \right\} = \left[\begin{array}{ccc} 0 & \kappa_2 & -\kappa_1 \\ -\kappa_2 & 0 & \kappa_3 \\ \kappa_1 & -\kappa_3 & 0 \end{array} \right] \left\{ \begin{array}{c} \mathbf{e_1} \\ \mathbf{e_2} \\ \mathbf{e_3} \end{array} \right\} \tag{5}$$

where $\kappa_1 = \kappa \sin\theta$, $\kappa_2 = \kappa \cos\theta$ and $\kappa_3 = \tau + \dfrac{d\theta}{ds}$.

The position vector of a generic point P within the beam domain can be defined as:

$$\boldsymbol{r}_P = \boldsymbol{r}(s) + \xi\,\boldsymbol{e}_2 + \eta\,\boldsymbol{e}_3 \tag{6}$$

being $\{s, \xi, \eta\}$ the coordinates associated to the $\{\mathbf{e_1}, \mathbf{e_2}, \mathbf{e_3}\}$ reference system. Finally, from Eq. (6), the expressions for the determinant of the metric tensor g and the infinitesimal volume dV can be derived (see Washizu [28]):

$$g = (1 - \xi\kappa_2 + \eta\kappa_1)^2 \tag{7}$$

$$dV = H\ ds\ d\xi\ d\eta \tag{8}$$

where $H = \sqrt{g}$.

In this study, $\boldsymbol{e}_2$ and $\boldsymbol{e}_3$ vectors are assumed to coincide with $\boldsymbol{n}$ and $\boldsymbol{b}$ (i.e. $\theta = 0°$), therefore $\kappa_1 = 0$, $\kappa_2 = \kappa$ and $\kappa_3 = \tau$. Furthermore, a constant radius of curvature R and no twist of the beam axis are considered ($\kappa = 1/R$ and $\tau = 0$).

2.2 Strain-displacement relations

The displacement vector expressed in the local reference system is:

$$\mathbf{u}^T(s, \xi, \eta) = \left\{\ u_s(s, \xi, \eta)\quad u_\xi(s, \xi, \eta)\quad u_\eta(s, \xi, \eta)\ \right\} \tag{9}$$

where superscript "T" represents the transposition operator.

The strain vector $\boldsymbol{\varepsilon}$ is given by:

$$\boldsymbol{\varepsilon}^T = \left\{\ \varepsilon_{ss}\quad \varepsilon_{\xi\xi}\quad \varepsilon_{\eta\eta}\quad \varepsilon_{\xi\eta}\quad \varepsilon_{s\eta}\quad \varepsilon_{s\xi}\ \right\} \tag{10}$$

6

Under the hypothesis of geometrical linearity, the strain-displacement relations are given by the following relations:

$$\varepsilon_{ss} = \frac{1}{H}\left(\frac{\partial u_s}{\partial s} - \kappa u_\xi\right)$$
$$\varepsilon_{\xi\xi} = \frac{\partial u_\xi}{\partial \xi}$$
$$\varepsilon_{\eta\eta} = \frac{\partial u_\eta}{\partial \eta}$$
$$\varepsilon_{\xi\eta} = \frac{\partial u_\xi}{\partial \eta} + \frac{\partial u_\eta}{\partial \xi} \tag{11}$$
$$\varepsilon_{s\eta} = \frac{1}{H}\left(\frac{\partial u_\eta}{\partial s}\right) + \frac{\partial u_s}{\partial \eta}$$
$$\varepsilon_{s\xi} = \frac{1}{H}\left(\frac{\partial u_\xi}{\partial s} + \kappa u_s\right) + \frac{\partial u_s}{\partial \xi}$$

Eqs. (11) can be written in a matrix form as follows:

$$\boldsymbol{\varepsilon} = \left(\mathbf{D}_s + \mathbf{D}_\Omega + \mathbf{D}_\kappa\right)\mathbf{u} \tag{12}$$

$\mathbf{D}_s$, $\mathbf{D}_\Omega$ and $\mathbf{D}_\kappa$ are the following differential matrix operators:

$$\mathbf{D}_s = \begin{bmatrix} \frac{1}{H}\frac{\partial}{\partial s} & 0 & 0 \\ 0 & 0 & 0 \\ 0 & 0 & 0 \\ 0 & 0 & 0 \\ 0 & 0 & \frac{1}{H}\frac{\partial}{\partial s} \\ 0 & \frac{1}{H}\frac{\partial}{\partial s} & 0 \end{bmatrix} \quad \mathbf{D}_\Omega = \begin{bmatrix} 0 & 0 & 0 \\ 0 & \frac{\partial}{\partial \xi} & 0 \\ 0 & 0 & \frac{\partial}{\partial \eta} \\ 0 & \frac{\partial}{\partial \eta} & \frac{\partial}{\partial \xi} \\ \frac{\partial}{\partial \eta} & 0 & 0 \\ \frac{\partial}{\partial \xi} & 0 & 0 \end{bmatrix} \quad \mathbf{D}_\kappa = \begin{bmatrix} 0 & -\frac{\kappa}{H} & 0 \\ 0 & 0 & 0 \\ 0 & 0 & 0 \\ 0 & 0 & 0 \\ 0 & 0 & 0 \\ \frac{\kappa}{H} & 0 & 0 \end{bmatrix} \tag{13}$$

$\mathbf{D}_s$ is the differential operator accounting for the derivative along the beam axis, $\mathbf{D}_\Omega$ for the cross-sectional variations and $\mathbf{D}_\kappa$ includes the curvature term.

2.3 Constitutive equations

Accordingly to the strain vector definition, the stress vector $\boldsymbol{\sigma}$ is given by:

$$\boldsymbol{\sigma}^T = \left\{ \begin{matrix} \sigma_{ss} & \sigma_{\xi\xi} & \sigma_{\eta\eta} & \sigma_{\xi\eta} & \sigma_{s\eta} & \sigma_{s\xi} \end{matrix} \right\} \tag{14}$$

In the case of a linear elastic material, Hooke's law reads:

$$\boldsymbol{\sigma} = \mathbf{C}\,\boldsymbol{\varepsilon} \tag{15}$$

where $\mathbf{C}$ is the material elastic stiffness matrix:

$$
\mathbf{C} = \begin{bmatrix}
C_{11} & C_{12} & C_{13} & 0 & 0 & 0 \\
C_{12} & C_{22} & C_{23} & 0 & 0 & 0 \\
C_{13} & C_{23} & C_3 & 0 & 0 & 0 \\
0 & 0 & 0 & C_{44} & 0 & 0 \\
0 & 0 & 0 & 0 & C_{55} & 0 \\
0 & 0 & 0 & 0 & 0 & C_{66}
\end{bmatrix}
\tag{16}
$$

For isotropic materials, the dependency of the coefficients C_{ij} versus Young's modulus E and Poisson's ratio ν is given by:

$$
\begin{aligned}
C_{11} = C_{22} = C_{33} &= \frac{1 - \nu}{(1 + \nu)(1 - 2\nu)} E \\
C_{12} = C_{13} = C_{23} &= \frac{\nu}{(1 + \nu)(1 - 2\nu)} E \\
C_{44} = C_{55} = C_{66} &= \frac{1}{2(1 + \nu)} E
\end{aligned}
\tag{17}
$$

3 Unified Formulation

The displacement field is a priori assumed over the cross-section in the following manner:

$$
\mathbf{u}(\xi, \eta, s) = F_\tau(\xi, \eta)\, \mathbf{u}_\tau(s) \quad \text{with} \quad \tau = 1,\, 2,\, \ldots,\, N_u
\tag{18}
$$

According to Einstein's notation, a repeated index τ implicitly represents a summation. $F_\tau(\xi, \eta)$ is a generic expansion function over the cross-section, N_u is the number of accounted terms and $\mathbf{u}_\tau = \{u_{s\tau}\ u_{\xi\tau}\ u_{\eta\tau}\}^T$.

Since the choice of the expansion functions $F_\tau(\xi, \eta)$ and N_u is arbitrary, several displacement-based beam theories can be derived and investigated within the same formulation. In this work, two different classes of expansion functions $F_\tau(\xi, \eta)$ are used: Taylor Expansions (TE) and Hierarchical Legendre Expansions (HLE).

3.1 Taylor expansions

The generic explicit form of the displacement field expanded via N-order Taylor polynomials is given by:

$$
\begin{aligned}
u_s &= u_{s1} + u_{s2}\xi + u_{s3}\eta + \cdots + u_{s\frac{(N^2+N+2)}{2}}\xi^N + \cdots + u_{s\frac{(N+1)(N+2)}{2}}\eta^N \\
u_\xi &= u_{\xi 1} + u_{\xi 2}\xi + u_{\xi 3}\eta + \cdots + u_{\xi\frac{(N^2+N+2)}{2}}\xi^N + \cdots + u_{\xi\frac{(N+1)(N+2)}{2}}\eta^N \\
u_\eta &= u_{\eta 1} + u_{\eta 2}\xi + u_{\eta 3}\eta + \cdots + u_{\eta\frac{(N^2+N+2)}{2}}\xi^N + \cdots + u_{\eta\frac{(N+1)(N+2)}{2}}\eta^N
\end{aligned}
\tag{19}
$$

In the framework of CUF notation introduced in Eq. (18), N_u and F_τ can be expressed as function of the order of the approximating polynomials N through Pascal's triangle in Table 1.

8

3.2 Hierarchical Legendre expansions

A HLE-based cross-sectional displacement field is defined through the use of vertex, edge and internal cross-sectional polynomials. The vertex polynomials correspond to the bi-linear Lagrange polynomials:

$$F_\tau(\zeta_1, \zeta_2) = \frac{1}{4}(1 - \zeta_{1\tau}\zeta_1)(1 - \zeta_{2\tau}\zeta_2) \quad \text{with} \quad \tau = 1, 2, 3, 4 \tag{20}$$

being ζ_1, ζ_2 the natural cross-section coordinates varying from -1 to 1 and $\zeta_{1\tau}$, $\zeta_{2\tau}$ the cross-section vertex coordinates. Edge polynomials are used for polynomial degrees $p \geq 2$ and they are defined as:

$$\begin{aligned}
F_\tau(\zeta_1, \zeta_2) &= \frac{1}{2}(1 - \zeta_2)\phi_p(\zeta_1) \quad \text{with} \quad \tau = 5, 9, 13, 18, ... \\
F_\tau(\zeta_1, \zeta_2) &= \frac{1}{2}(1 + \zeta_1)\phi_p(\zeta_2) \quad \text{with} \quad \tau = 6, 10, 14, 19, ... \\
F_\tau(\zeta_1, \zeta_2) &= \frac{1}{2}(1 + \zeta_2)\phi_p(\zeta_1) \quad \text{with} \quad \tau = 7, 11, 15, 20, ... \\
F_\tau(\zeta_1, \zeta_2) &= \frac{1}{2}(1 - \zeta_1)\phi_p(\zeta_2) \quad \text{with} \quad \tau = 8, 12, 16, 21, ...
\end{aligned} \tag{21}$$

where:

$$\phi_p(\zeta_1) = \sqrt{\frac{2p-1}{p}} \int_{-1}^{\zeta_1} L_{p-1}(x)\, dx \tag{22}$$

being L_{p-1} a 1D Legendre polynomial of order $p-1$ and $\phi_p(\zeta_2)$ being defined in an analogous manner as $\phi_p(\zeta_1)$ in Eq. (22). Finally, for $p \geq 4$, internal cross-sectional polynomials are also taken into account. As an example, for $p = 6$, the following additional expansion functions are considered:

$$\begin{aligned}
F_{28}(\zeta_1, \zeta_2) &= \phi_4(\zeta_1)\phi_2(\zeta_2) \\
F_{29}(\zeta_1, \zeta_2) &= \phi_3(\zeta_1)\phi_3(\zeta_2) \\
F_{30}(\zeta_1, \zeta_2) &= \phi_2(\zeta_1)\phi_4(\zeta_2)
\end{aligned} \tag{23}$$

The relation between the polynomial degree p and the number of expansion functions taken into account in the displacement field is shown in Fig. 2 for polynomials up to the 7-th order. For more details, a thorough presentation of HLE-based beam theories can be found in Carrera et al. [23] and Pagani et al. [25].

3.3 Strain field

According to Eq. (11) and (18), the strain-displacement relations become:

$$\begin{aligned}
\varepsilon_{ss} &= \frac{F_\tau}{H}(u_{s\tau,s} - \kappa u_{\xi\tau}) \\
\varepsilon_{\xi\xi} &= F_{\tau,\xi}u_{\xi\tau} \\
\varepsilon_{\eta\eta} &= F_{\tau,\eta}u_{\eta\tau} \\
\varepsilon_{\xi\eta} &= F_{\tau,\eta}u_{\xi\tau} + F_{\tau,\xi}u_{\eta\tau} \\
\varepsilon_{s\eta} &= \frac{1}{H}F_\tau u_{\eta\tau,s} + F_{\tau,\eta}u_{s\tau} \\
\varepsilon_{s\xi} &= \frac{F_\tau}{H}(u_{\xi\tau,s} + \kappa u_{s\tau}) + F_{\tau,\xi}u_{s\tau}
\end{aligned} \tag{24}$$

9

where the subscripts 's', 'ξ' and 'η', when preceded by comma, represent derivation versus the respective coordinate.

4   Governing Equations

For both strong and weak form solutions, the governing equations for a static mechanical analysis are obtained via the PVD:

$$\delta L_{\text{int}} = \delta L_{\text{ext}} \tag{25}$$

L_{int} represents the strain energy, L_{ext} the external work and δ stands for a virtual variation.

4.1   Strong form Navier-type solution

Governing differential equations and boundary conditions are obtained through the application of PVD. The virtual variation of the beam strain energy is given by:

$$\delta L_{\text{int}} = \int_l \int_\Omega \delta \boldsymbol{\epsilon}^T \boldsymbol{\sigma} H(\xi) ds d\xi d\eta \tag{26}$$

where l corresponds to the total length of the curved axis and Ω is the beam cross-section area. By considering the geometrical relations in Eqs. (12), the constitutive relations in Eqs. (15) and the displacements unified formulation in Eq. (18), the compact vectorial form of the virtual variation of the strain energy in terms of displacement components is given by:

$$\delta L_{\text{int}} = \int_l \delta \mathbf{u}_t^T \overline{\mathbf{K}}^{\tau t} \mathbf{u}_\tau ds + \delta \mathbf{u}_t^T \overline{\mathbf{\Pi}}^{\tau t} \mathbf{u}_\tau \big|_{s=0}^{s=l} \tag{27}$$

Subscript t has the same meaning of subscript τ introduced in Eq. (18), but it is here referred to the virtual displacement vector. $\overline{\mathbf{K}}^{\tau t}$ represents the differential stiffness matrix fundamental nucleus and $\overline{\mathbf{\Pi}}^{\tau t}$ is the differential fundamental nucleus related to the boundary conditions. Once the approximation order of the displacement field is fixed, the governing equations and the boundary conditions of the desired model can be obtained via assembly of the respective nucleus over the indexes τ and t.

The variation of the virtual external work done by the transverse pressure loading p_ξ acting at $\xi = \overline{\xi}$ over an area $A_\xi : [0, l] \times [\overline{\eta}_1, \overline{\eta}_2]$ and the contribution of a transverse pressure p_η acting at $\eta = \overline{\eta}$ over the domain $A_\eta : [0, l] \times [\overline{\xi}_1, \overline{\xi}_2]$ can be written as:

$$\delta L_{\text{ext}} = \int_l \left(p_\xi E_t^{\overline{\xi}} \delta u_{\xi t} + p_\eta E_t^{\overline{\eta}} \delta u_{\eta t} \right) ds \tag{28}$$

where:

$$
\begin{aligned}
E_t^{\overline{\xi}} &= H\left(\overline{\xi}\right) \int_{\overline{\eta}_1}^{\overline{\eta}_2} F_t\left(\overline{\xi}, \eta\right) d\eta \\
E_t^{\overline{\eta}} &= \int_{\overline{\xi}_1}^{\overline{\xi}_2} H\left(\xi\right) F_t\left(\overline{\eta}, \xi\right) d\xi
\end{aligned}
\tag{29}
$$

10

For the sake of brevity, only transverse pressure components are reported within the formulation, but the contributions given by any generic surface loading can be derived in an analogous manner. A Navier-type harmonic displacement field is assumed along the curved axis coordinate in order to solve the differential equations and automatically satisfy the boundary conditions for simply supported beams:

$$
\begin{aligned}
u_{s\tau} &= U_{s\tau}\cos(\alpha s) \\
u_{\xi\tau} &= U_{\xi\tau}\sin(\alpha s) \\
u_{\eta\tau} &= U_{\eta\tau}\sin(\alpha s)
\end{aligned}
\tag{30}
$$

where $\alpha = \frac{m\pi}{l}$, m is the number of half-waves along the beam axis and $\{U_{s\tau},\ U_{\xi\tau},\ U_{\eta\tau}\}$ are the generalised displacement unknowns that are obtained by solving the governing algebraic system. The applied transverse pressures p_ξ and p_η are also assumed to vary harmonically along the beam axis:

$$
\begin{aligned}
p_\xi &= P_\xi\sin(\alpha s) \\
p_\eta &= P_\eta\sin(\alpha s)
\end{aligned}
\tag{31}
$$

Without loss of generality, due to the linearity hypothesis between load and displacements, any loading profile can be obtained from Eq. (31) via Fourier's series expansion approximation (see Carrera and Giunta [29, 30]). Upon substitution of Eq. (29) and (31) into the governing differential equations, the algebraic stiffness matrix $\mathbf{K}^{\tau t}$ and the load vector $\mathbf{P}^t$ fundamental nuclei are obtained. Their complete expressions can be found in Appendix A.

4.2   Weak form FEM solution

With respect to the presented closed-form solution, CUF-based one-dimensional curved finite element solution has the main advantage to be suitable for the study of structural problems with arbitrary boundary conditions. On the other hand, it is well known that curved finite elements can show locking phenomena that negatively influence the accuracy of the results and, therefore, a closed-form exact analytical solution will prove useful for locking assessment purposes. The displacement variables are interpolated along the curved beam axis through conventional Lagrangian shape functions N_i:

$$
\mathbf{u}_\tau(s) = N_i(s)\,\mathbf{q}_{\tau i} \quad \text{with} \quad \tau = 1,\ 2,\ \ldots,\ N_u \quad \text{and} \quad i = 1,\ \ldots,\ N_n^e
\tag{32}
$$

where the subscript i represent implicit summations over the element nodes, $\mathbf{q}_{\tau i}$ is the unknown nodal displacement vector and N_n^e is the number of nodes per element. Cubic elements are used in the numerical analyses. The virtual variation of the element strain energy is given by:

$$
\delta L_{\text{int}} = \int_{l^e}\int_\Omega \delta\boldsymbol{\epsilon}^T\boldsymbol{\sigma}H(\xi)ds d\xi d\eta
\tag{33}
$$

being l^e the curved beam element length. If the finite element formulation in Eq. (32) is considered, along with Eqs. (12), (15) and (18), the virtual variation of the strain energy

11

can be written as:

$$\delta L_{\text{int}} = \delta \mathbf{q}_{tj}^T \mathbf{K}_e^{\tau tij} \mathbf{q}_{\tau i} \tag{34}$$

$\mathbf{K}_e^{\tau tij}$ is the element stiffness matrix fundamental nucleus. Analogously to the fundamental nuclei derived in the closed-form solution, $\mathbf{K}_e^{\tau tij}$ needs to be assembled over the indexes τ, t, i and j in order to obtain the element stiffness matrix of the desired higher-order beam element. The components of the element fundamental nucleus are explicitly reported in Appendix B. As far as the virtual variation of the element external work is concerned, the contributions given by the transverse pressure loadings p_ξ and p_η can be written as:

$$\delta L_{\text{ext}}^{p_\xi} = \delta q_{\xi tj} p_\xi I_j E_t^{\overline{\xi}} \quad \delta L_{\text{ext}}^{p_\eta} = \delta q_{\eta tj} p_\eta I_j E_t^{\overline{\eta}} \tag{35}$$

with:

$$I_j = \int_{l^e} N_j(s)\, ds \tag{36}$$

The contributions given by the line loads l_ξ and l_η applied at (ξ_l, η_l) are:

$$\delta L_{\text{ext}}^{l_\xi} = \delta q_{\xi tj} l_\xi I_j F_t(\xi_l, \eta_l) H(\xi_l) \quad \delta L_{\text{ext}}^{l_\eta} = \delta q_{\eta tj} l_\eta I_j F_t(\xi_l, \eta_l) H(\xi_l) \tag{37}$$

The contribution of a concentrated load $\mathbf{F}$ applied at (s_F, ξ_F, η_F) is given by:

$$\delta L_{\text{ext}}^F = F_t(\xi_F, \eta_F) N_j(s_F) \delta \mathbf{q}_{tj}^T \mathbf{F} \tag{38}$$

Finally, the virtual variation of the external work can be written as the summation of each contribution:

$$\delta L_{\text{ext}} = \delta L_{\text{ext}}^{p_\xi} + \delta L_{\text{ext}}^{p_\eta} + \delta L_{\text{ext}}^{l_\xi} + \delta L_{\text{ext}}^{l_\eta} + \delta L_{\text{ext}}^F \tag{39}$$

4.2.1 Shear and membrane locking: MITC beam elements

The numerical phenomenon of locking is a major issue in the structural analysis of curved bodies. This detrimental phenomenon needs to be mitigated, especially when slender structures and low-order shape functions are considered. By using the MITC method, locking phenomena can be alleviated by interpolating the axial and shear strain components along the beam element axis in the following manner:

$$\begin{aligned} \overline{\varepsilon}_{ss} &= \overline{N}_m \varepsilon_{ss}^m \\ \overline{\varepsilon}_{s\eta} &= \overline{N}_m \varepsilon_{s\eta}^m \\ \overline{\varepsilon}_{s\xi} &= \overline{N}_m \varepsilon_{s\xi}^m \end{aligned} \tag{40}$$

where m denotes an implicit summation and varies from 1 to $N_n^e - 1$. ε_{ss}^m, $\varepsilon_{s\eta}^m$ and $\varepsilon_{s\xi}^m$ are the strain components coming from the geometrical relations in Eq. (11) evaluated at the m-th tying point and $\overline{N}_m$ are the assumed interpolating functions. For cubic elements, their expressions as functions of the natural beam element coordinate r are given by:

$$\overline{N}_1 = \tfrac{5}{6} r \left(r - \sqrt{\tfrac{3}{5}} \right) \quad \overline{N}_2 = -\tfrac{5}{3} \left(r - \sqrt{\tfrac{3}{5}} \right) \left(r + \sqrt{\tfrac{3}{5}} \right) \quad \overline{N}_3 = \tfrac{5}{6} r \left(r + \sqrt{\tfrac{3}{5}} \right) \tag{41}$$

whereas the tying points coordinates are: $r_{T1} = -\sqrt{\frac{3}{5}}$, $r_{T2} = 0$ and $r_{T3} = \sqrt{\frac{3}{5}}$. The new estimate for the strain components given by Eq. (40) is used within the constitutive relations in Eq. (15) as well as for the evaluation of the element strain energy given by Eq. (33). The explicit expression of the fundamental nucleus for the MITC beam element can be found in the companion paper [31].

5   Numerical Results

The beam support is $[0, l] \times [-h/2, h/2] \times [-b/2, b/2]$ with l being the length, h the thickness and b the width. The geometrical features of the considered structure are shown in Figure 3. Simply supported, cantilever and doubly-clamped circular beams are investigated for different in-plane and out-of-plane loading configurations and slenderness ratios. Beams made of aluminium are considered ($E = 30$ GPa and $\nu = 0.17$). Results provided by the proposed family of advanced curved beam models are compared with commercial software finite elements solutions as well as elasticity solutions and results available in the literature.

5.1   Locking assessment

In order to assess the behaviour of the present formulation in terms of locking, a plane stress analysis of simply supported circular arches for different slenderness ratios is carried out via standard cubic elements, referred to as B4, and MITC cubic elements, referred to as MITC4. An exact Navier-type solution, obtained with $m = 150$ half-waves, is used as reference. The opening angle of the beam is $\Phi = \frac{2}{3}\pi$, the thickness $h = 0.6$ m and the width $b = 0.4$ m. A uniform pressure $p_\xi = 1$ Pa is applied at the top surface of the beam ($\xi = h/2$). The variation of $\hat{u}_z = u_z^{\text{FEM}}/u_z^{\text{Nav}}$ versus the slenderness ratio l/h by using four beam elements is shown in Figure 4. A TE2 beam model has been used for the presented results, nevertheless the effectiveness of the MITC method for locking mitigation does not depend upon the order of the theory nor the approximation base type. Tables 2 and 3 show the convergence analysis of the transverse displacement at ($s = l/2, \xi = 0$) for a very thick beam ($l/h = 5$) and a very slender one ($l/h = 1000$), respectively. Excellent rates of convergence can be observed for the MITC beam elements.

5.2   Circular thick arch

A plane stress analysis for the displacement and stress fields prediction in thick curved beams with circular axis is carried out in this section. Two-dimensional finite elements validation has been obtained via bi-quadratic 8-node "Plane183" Ansys elements. As far as the computational costs are concerned, the most refined beam theory considered are HL5 and TE5, with number of degrees of freedom (N_{DOFs}) equal to 12, for the analytical solution, and 1452, for a 121 nodes finite elements solution, whereas N_{DOFs} for the two-dimensional model used for comparison (120×24 elements) is 70274.

5.2.1 Simply supported beam

The beam has a rectangular cross-section with $h = 0.6$ m and $b = 0.4$ m. The circular axis has radius of curvature $R = 4$ m and opening angle $\Phi = 2/3\pi$. Results provided by the proposed finite elements are compared with the corresponding Navier-type solution, which represents an exact solution in the framework of the theory. For the sake of completeness, both TE and HLE expansions are reported, although, for homogeneous material structures under plane stress conditions, no significant differences can be noticed. Table 4 shows the maximum tangential and radial displacements for a uniform bending pressure load $p_\xi = 1$ Pa applied at the top surface ($\xi = h/2$). The evaluation points are ($s = 0$, $\xi = -h/2$) for u_s and ($s = l/2$, $\xi = 0$) for u_ξ. Figures 5 to 7 show the agreement between strong form and weak form solutions for the through-the-thickness profile of axial, radial and shear stresses.

5.2.2 Clamped-clamped beam

Doubly-clamped boundary conditions are considered in this section and different loading cases are investigated. Geometrical properties are the same as in the previous section. Results obtained via the proposed finite elements are compared with those provided by Tupecki and Arpaci [3] and Litewka and Rakowski [10], as well as Ansys 2D elements. A case of a concentrated force $F = 1000$ N applied at ($s = l/2$, $\xi = 0$) is considered as well as the case of a uniform load per unit length $p_\xi b = 1000$ N/m applied at $\xi = 0$, in accordance with [10]. Table 5 shows the dimensionless displacements $\tilde{u} = u/l$ evaluated at the point ($s = l/2$, $\xi = -h/2$). Results show that the proposed advanced beam models allow a more accurate prediction of the displacement field with respect to the classical theories, when compared to the reference 2D finite element solution. Since higher-order theories implicitly account for shear deformation effects as well as local cross-sectional warping, the errors can be reduced from 1.3% to 0.08% for the case of concentrated radial force and from 3.3% to 0.3% for the case of concentrated axial force.

5.2.3 Cantilever beam

In this section, stress results for a cantilever circular beam with $R = 1$ m, $\Phi = \pi/2$ and square cross-section ($h = b = l/10$) are compared with elasticity solutions given by Timoshenko and Goodier [1]. The load is a concentrated radial force $F_\xi = 1$ N at the free end ($s = l$, $\xi = 0$). Figures 8 to 10 show the variation of the dimensionless axial, radial and shear stresses $\tilde{\sigma} = \sigma bh/(F_\xi \sqrt{2})$ along the dimensionless thickness coordinate $\tilde{\xi} = \xi/h$ at the mid-span of the beam axis ($s = l/2$). Results show that the exact stress distributions can be provided by higher-order theories such as TE5.

5.3 3D balcony

A semi-circular 3D balcony is considered for the last assessment. This case study focuses on the capabilities of higher-order curved beam elements to provide an accurate prediction of

the displacement and stress fields in a more general three-dimensional case with out-of-plane loadings. The radius R is equal to 3 m, whereas the opening angle $\Phi = \pi$. The cross section is square with dimensions $h = b = 0.3$ m. The structure is clamped at both end sides and a line load of magnitude $l_\eta = 5$ kN/m is applied along the axis, as shown in Figure 11. Two different mesh discretizations with 10 and 20 MITC4 beam elements have been considered. As far as the beam cross-section kinematics is concerned, polynomial expansions based on HLE are investigated. The full three-dimensional formulation is considered and resuls are compared with Abaqus "C3D8" quadratic brick elements.

As far as the computational costs are concerned, the N_{DOFs} for the most refined one-dimensional model used in the following analyses (HL5 beam theory and 61 nodes), is 4209, whereas, for the three-dimensional model used for comparison ($200 \times 10 \times 10$ elements), N_{DOFs} is 278223. Figure 12 shows the transverse displacement along the arc-length coordinate s for Legendre polynomial expansions up to the 3rd-order. The solutions provided by Zhang et al. [16] as well as solid Abaqus model are included for comparison purposes. Figures 13 and 14 show the axial and transverse shear stresses profiles at different locations within the structure. For both displacements and stresses, the accuracy of the solutions can be greatly increased by enriching the kinematics of the beam with higher-order terms. Indeed, for this case, a 3rd-order model HL3 is already capable to predict the stress fields with solid-like accuracy. For the sake of completeness, the 3D colour plots for the axial stress σ_{ss}, transverse shear stresses $\sigma_{s\eta}$ and $\sigma_{s\xi}$ provided by the fifth order model HL5 are presented in Figures 15, 16 and 17, respectively.

6   Conclusions

A family of one-dimensional beam models based on CUF has been derived for the mechanical analysis of curved beam structures. Different geometries, boundary conditions and loading cases have been investigated by a strong form Navier-type solution as well as a weak form solution based on the finite element method. For the latter, locking phenomena have been assessed against exact solutions and MITC method was proven to yield excellent convergence rates: 4 MITC cubic elements instead of 40 standard cubic elements were needed in order to predict the exact radial displacement in slender beams. Results in terms of displacement and stress profiles over the whole beam domain were compared with commercial software FEM solutions, elasticity solutions and data from the existing literature. Unlike classical 1D models, higher-order theories such as TE3 or HL3 can accurately predict the axial, shear and radial stresses in thick curved beam-like structures, with computational costs differing by one or two orders of magnitude when compared to 2D and 3D commercial software finite elements.

A Closed-form fundamental nuclei

The components of the differential stiffness matrix $\overline{\mathbf{K}}^{\tau t}$ introduced in Eq. (27) are reported below:

$$\overline{K}^{\tau t}_{ss} = -J^{11}_{\tau t\frac{1}{H}}\frac{\partial^2}{\partial s^2} + J^{55}_{\tau,\eta t,\eta H} + J^{66}_{\tau,\xi t,\xi H} + \kappa\left(J^{66}_{\tau t,\xi} + J^{66}_{\tau,\xi t}\right) + \kappa^2 J^{66}_{\tau t\frac{1}{H}}$$

$$\overline{K}^{\tau t}_{s\xi} = \left[-J^{12}_{\tau,\xi t} + J^{66}_{\tau t,\xi} + \kappa\left(J^{66}_{\tau t\frac{1}{H}} + J^{11}_{\tau t\frac{1}{H}}\right)\right]\frac{\partial}{\partial s}$$

$$\overline{K}^{\tau t}_{s\eta} = \left(-J^{13}_{\tau,\eta t} + J^{55}_{\tau t,\eta}\right)\frac{\partial}{\partial s}$$

$$\overline{K}^{\tau t}_{\xi s} = \left[J^{12}_{\tau t,\xi} - J^{66}_{\tau,\xi t} - \kappa\left(J^{66}_{\tau t\frac{1}{H}} + J^{11}_{\tau t\frac{1}{H}}\right)\right]\frac{\partial}{\partial s}$$

$$\overline{K}^{\tau t}_{\xi\xi} = J^{22}_{\tau,\xi t,\xi H} + J^{44}_{\tau,\eta t,\eta H} - J^{66}_{\tau t\frac{1}{H}}\frac{\partial^2}{\partial s^2} - \kappa\left(J^{12}_{\tau t,\xi} + J^{12}_{\tau,\xi t}\right) + \kappa^2 J^{11}_{\tau t\frac{1}{H}} \qquad (42)$$

$$\overline{K}^{\tau t}_{\xi\eta} = J^{23}_{\tau,\eta t,\xi H} + J^{44}_{\tau,\xi t,\eta H} - \kappa J^{13}_{\tau,\eta t}$$

$$\overline{K}^{\tau t}_{\eta s} = \left(J^{13}_{\tau t,\eta} - J^{55}_{\tau,\eta t}\right)\frac{\partial}{\partial s}$$

$$\overline{K}^{\tau t}_{\eta\xi} = J^{23}_{\tau,\xi t,\eta H} + J^{44}_{\tau,\eta t,\xi H} - \kappa J^{13}_{\tau t,\eta}$$

$$\overline{K}^{\tau t}_{\eta\eta} = J^{33}_{\tau,\eta t,\eta H} + J^{44}_{\tau,\xi t,\xi H} - J^{55}_{\tau t\frac{1}{H}}\frac{\partial^2}{\partial s^2}$$

being $J^{gh}_{\tau_{(,\phi)}t_{(,\psi)}}$, $J^{gh}_{\tau_{(,\phi)}t_{(,\psi)}H}$ and $J^{gh}_{\tau_{(,\phi)}t_{(,\psi)}\frac{1}{H}}$ the following integrals over the beam cross-section Ω:

$$J^{gh}_{\tau_{(,\phi)}t_{(,\psi)}} = \int_{\Omega} C_{gh}F_{\tau_{(,\phi)}}F_{t_{(,\psi)}}\, d\xi\, d\eta$$

$$J^{gh}_{\tau_{(,\phi)}t_{(,\psi)}H} = \int_{\Omega} C_{gh}F_{\tau_{(,\phi)}}F_{t_{(,\psi)}}H\, d\xi\, d\eta \qquad (43)$$

$$J^{gh}_{\tau_{(,\phi)}t_{(,\psi)}\frac{1}{H}} = \int_{\Omega} C_{gh}F_{\tau_{(,\phi)}}F_{t(,\psi)}\frac{1}{H}\, d\xi\, d\eta$$

As far as the boundary conditions are concerned, the components of $\overline{\mathbf{\Pi}}^{\tau t}$ are:

$$\overline{\Pi}^{\tau t}_{ss} = J^{11}_{\tau t\frac{1}{H}}\frac{\partial}{\partial s} \qquad\qquad \overline{\Pi}^{\tau t}_{s\xi} = J^{12}_{\tau,\xi t} - \kappa J^{11}_{\tau t\frac{1}{H}} \qquad \overline{\Pi}^{\tau t}_{s\eta} = J^{13}_{\tau,\eta t}$$

$$\overline{\Pi}^{\tau t}_{\xi s} = J^{66}_{\tau,\xi t} + \kappa J^{66}_{\tau t\frac{1}{H}} \qquad \overline{\Pi}^{\tau t}_{\xi\xi} = J^{66}_{\tau t\frac{1}{H}}\frac{\partial}{\partial s} \qquad\qquad \overline{\Pi}^{\tau t}_{\xi\eta} = 0 \qquad (44)$$

$$\overline{\Pi}^{\tau t}_{\eta s} = J^{55}_{\tau,\eta t} \qquad\qquad \overline{\Pi}^{\tau t}_{\eta\xi} = 0 \qquad\qquad \overline{\Pi}^{\tau t}_{\eta\eta} = J^{55}_{\tau t\frac{1}{H}}\frac{\partial}{\partial s}$$

Therefore, the explicit form of the boundary conditions is given by:

$$\delta u_{st}\left[J^{11}_{\tau t\frac{1}{H}}u_{s\tau,s} + \left(J^{12}_{\tau,\xi t} - \kappa J^{11}_{\tau t\frac{1}{H}}\right)u_{\xi\tau} + J^{13}_{\tau,\eta t}u_{\eta\tau}\right]\Big|^{s=l}_{s=0} = 0$$

$$\delta u_{\xi t}\left[\left(J^{66}_{\tau,\xi t} + \kappa J^{66}_{\tau t\frac{1}{H}}\right)u_{s\tau} + J^{66}_{\tau t\frac{1}{H}}u_{\xi\tau,s}\right]\Big|^{s=l}_{s=0} = 0 \qquad (45)$$

$$\delta u_{\eta t}\left[J^{55}_{\tau,\eta t}u_{s\tau} + J^{55}_{\tau t\frac{1}{H}}u_{\eta\tau,s}\right]\Big|^{s=l}_{s=0} = 0$$

16

If the displacement field in Eq. (29) is adopted, the boundary conditions are satisfied for simply supported beams, since:

$$
\begin{aligned}
u_{s\tau,s}\left(0\right) &= u_{s\tau,s}\left(l\right) = 0 \\
u_{\xi\tau}\left(0\right) &= u_{\xi\tau}\left(l\right) = 0 \\
u_{\eta\tau}\left(0\right) &= u_{\eta\tau}\left((l\right) = 0
\end{aligned}
\tag{46}
$$

$$
\begin{aligned}
\delta u_{st,s}\left(0\right) &= \delta u_{st,s}\left(l\right) = 0 \\
\delta u_{\xi t}\left(0\right) &= \delta u_{\xi t}\left(l\right) = 0 \\
\delta u_{\eta t}\left(0\right) &= \delta u_{\eta t}\left((l\right) = 0
\end{aligned}
\tag{47}
$$

and the following algebraic stiffness matrix fundamental nucleus $\mathbf{K}^{\tau t}$ is obtained:

$$
\begin{aligned}
K_{ss}^{\tau t} &= \alpha^2 J_{\tau t \frac{1}{H}}^{11} + J_{\tau,\eta t,\eta H}^{55} + J_{\tau,\xi t,\xi H}^{66} + \kappa\left(J_{\tau t,\xi}^{66} + J_{\tau,\xi t}^{66}\right) + \kappa^2 J_{\tau t \frac{1}{H}}^{66} \\
K_{s\xi}^{\tau t} &= \alpha\left[-J_{\tau,\xi t}^{12} + J_{\tau t,\xi}^{66} + \kappa\left(J_{\tau t \frac{1}{H}}^{66} + J_{\tau t \frac{1}{H}}^{11}\right)\right] \\
K_{s\eta}^{\tau t} &= \alpha\left(-J_{\tau,\eta t}^{13} + J_{\tau t,\eta}^{55}\right) \\
K_{\xi s}^{\tau t} &= \alpha\left[-J_{\tau t,\xi}^{12} + J_{\tau,\xi t}^{66} + \kappa\left(J_{\tau t \frac{1}{H}}^{66} + J_{\tau t \frac{1}{H}}^{11}\right)\right] \\
K_{\xi\xi}^{\tau t} &= J_{\tau,\xi t,\xi H}^{22} + J_{\tau,\eta t,\eta H}^{44} + \alpha^2 J_{\tau t \frac{1}{H}}^{66} - \kappa\left(J_{\tau t,\xi}^{12} + J_{\tau,\xi t}^{12}\right) + \kappa^2 J_{\tau t \frac{1}{H}}^{11} \\
K_{\xi\eta}^{\tau t} &= J_{\tau,\eta t,\xi H}^{23} + J_{\tau,\xi t,\eta H}^{44} - \kappa J_{\tau,\eta t}^{13} \\
K_{\eta s}^{\tau t} &= \alpha\left(-J_{\tau t,\eta}^{13} + J_{\tau,\eta t}^{55}\right) \\
K_{\eta\xi}^{\tau t} &= J_{\tau,\xi t,\eta H}^{23} + J_{\tau,\eta t,\xi H}^{44} - \kappa J_{\tau t,\eta}^{13} \\
K_{\eta\eta}^{\tau t} &= J_{\tau,\eta t,\eta H}^{33} + J_{\tau,\xi t,\xi H}^{44} + \alpha^2 J_{\tau t \frac{1}{H}}^{55}
\end{aligned}
\tag{48}
$$

Once the displacement approximation order has been fixed, the stiffness matrix is straightforwardly obtained by summing the fundamental nucleus of Eqs. (48) for each term of the displacement expansion in Eq. (18).

As far as the load vector fundamental nucleus $\mathbf{P}^t$ is concerned, its non-zero components expression, according to Eq. (28), is given by:

$$
\begin{aligned}
P_\xi^t &= p_\xi E_t^{\overline{\xi}} \\
P_\eta^t &= p_\eta E_t^{\overline{\eta}}
\end{aligned}
\tag{49}
$$

B FEM fundamental nuclei

The components of the stiffness matrix fundamental nucleus $\mathbf{K}_e^{\tau t i j} \in \mathbb{R}^{3 \times 3}$ of the curved beam element are:

$$
\begin{aligned}
K_{ess}^{\tau t i j} &= I_{i,s j,s} J_{\tau t \frac{1}{H}}^{11} + I_{ij}\left(J_{\tau,\eta t,\eta H}^{55} + J_{\tau,\xi t,\xi H}^{66}\right) + \kappa I_{ij}\left(J_{\tau t,\xi}^{66} + J_{\tau,\xi t}^{66}\right) + \kappa^2 I_{ij} J_{\tau t \frac{1}{H}}^{66} \\
K_{es\xi}^{\tau t i j} &= I_{ij,s} J_{\tau,\xi t}^{12} + I_{i,sj} J_{\tau t,\xi}^{66} + \kappa\left(I_{i,sj} J_{\tau t \frac{1}{H}}^{66} - I_{ij,s} J_{\tau t \frac{1}{H}}^{11}\right) \\
K_{es\eta}^{\tau t i j} &= I_{ij,s} J_{\tau,\eta t}^{13} + I_{i,sj} J_{\tau t,\eta}^{55} \\
K_{e\xi s}^{\tau t i j} &= I_{i,sj} J_{\tau t,\xi}^{12} + I_{ij,s} J_{\tau,\xi t}^{66} + \kappa\left(I_{ij,s} J_{\tau t \frac{1}{H}}^{66} - I_{i,sj} J_{\tau t \frac{1}{H}}^{11}\right) \\
K_{e\xi\xi}^{\tau t i j} &= I_{ij}\left(J_{\tau,\xi t,\xi H}^{22} + J_{\tau,\eta t,\eta H}^{44}\right) + I_{i,sj,s} J_{\tau t \frac{1}{H}}^{66} - \kappa I_{ij}\left(J_{\tau t,\xi}^{12} + J_{\tau,\xi t}^{12}\right) + \kappa^2 I_{ij} J_{\tau t \frac{1}{H}}^{11} \qquad (50) \\
K_{e\xi\eta}^{\tau t i j} &= I_{ij}\left(J_{\tau,\eta t,\xi H}^{23} + J_{\tau,\xi t,\eta H}^{44}\right) - \kappa I_{ij} J_{\tau,\eta t}^{13} \\
K_{e\eta s}^{\tau t i j} &= I_{i,sj} J_{\tau t,\eta}^{13} + I_{ij,s} J_{\tau,\eta t}^{55} \\
K_{e\eta\xi}^{\tau t i j} &= I_{ij}\left(J_{\tau,\xi t,\eta H}^{23} + J_{\tau,\eta t,\xi H}^{44}\right) - \kappa I_{ij} J_{\tau t,\eta}^{13} \\
K_{e\eta\eta}^{\tau t i j} &= I_{ij}\left(J_{\tau,\eta t,\eta H}^{33} + J_{\tau,\xi t,\xi H}^{44}\right) + I_{i,sj,s} J_{\tau t \frac{1}{H}}^{55}
\end{aligned}
$$

where $I_{i_{(,s)} j_{(,s)}}$ is the following integral along the beam element axis:

$$
I_{i_{(,s)} j_{(,s)}} = \int_{l_e} N_{i_{(,s)}} N_{j_{(,s)}} \, ds \qquad (51)
$$

Subscript 's' preceded by comma represent derivation versus the axis coordinate. For a fixed approximation order, the element stiffness matrix has to be assembled according to the summation indexes τ, t, i and j.

Acknowledgements

References

[1] S. P. Timoshenko and J. N. Goodier. *Theory of elasticity*. McGraw-Hill, 1970.

[2] A. M. Yu and G. H. Nie. Explicit solutions for shearing and radial stresses in curved beams. *Mechanics Research Communications*, 32(3):323–331, 2005.

[3] E. Tufekci and A. Arpaci. Analytical solutions of in-plane static problems for non-uniform curved beams including axial and shear deformations. *Structural Engineering and Mechanics*, 22(2):131–150, 2006.

[4] L. Gimena, F. N. Gimena, and P. Gonzaga. Structural analysis of a curved beam element defined in global coordinates. *Engineering Structures*, 30(11):3355–3364, 2008.

[5] C. R. Babu and G. Prathap. A linear thick curved beam element. *International Journal for Numerical Methods in Engineering*, 23(7):1313–1328, 1986.

[6] B. Tabarrok, M. Farshad, and H. Yi. Finite element formulation of spatially curved and twisted rods. *Computer methods in applied mechanics and engineering*, 70(3):275–299, 1988.

[7] B. D. Reddy and M. B. Volpi. Mixed finite element methods for the circular arch problem. *Computer Methods in Applied Mechanics and Engineering*, 97(1):125–145, 1992.

[8] J. K. Choi and J. K. Lim. Simple curved shear beam elements. *International Journal for Numerical Methods in Biomedical Engineering*, 9(8):659–669, 1993.

[9] P. G. Lee and H. C. Sin. Locking-free curved beam element based on curvature. *International Journal for Numerical Methods in Engineering*, 37(6):989–1007, 1994.

[10] P. Litewka and J. Rakowski. The exact thick arch finite element. *Computers & Structures*, 68(4):369–379, 1998.

[11] P. Raveendranath, G. Singh, and G. Venkateswara Rao. A three-noded shear-flexible curved beam element based on coupled displacement field interpolations. *International Journal for Numerical Methods in Engineering*, 51(1):85–101, 2001.

[12] D. Zupan and M. Saje. Finite-element formulation of geometrically exact three-dimensional beam theories based on interpolation of strain measures. *Computer Methods in Applied Mechanics and Engineering*, 192(49):5209–5248, 2003.

[13] Z. H. Zhu and S. A. Meguid. Analysis of three-dimensional locking-free curved beam element. *International Journal of Computational Engineering Science*, 5(03):535–556, 2004.

[14] R. Nascimbene. An arbitrary cross section, locking free shear-flexible curved beam finite element. *International Journal for Computational Methods in Engineering Science and Mechanics*, 14(2):90–103, 2013.

[15] Y. Q. Tang, Z. H. Zhou, and S. L. Chan. An accurate curved beam element based on trigonometrical mixed polynomial function. *International Journal of Structural Stability and Dynamics*, 13(04):1250084, 2013.

[16] G. Zhang, R. Alberdi, and K. Khandelwal. Analysis of three-dimensional curved beams using isogeometric approach. *Engineering Structures*, 117:560–574, 2016.

[17] E. Carrera. Theories and finite elements for multilayered plates and shells: a unified compact formulation with numerical assessment and benchmarking. *Archives of Computational Methods in Engineering*, 10(3):216–296, 2003.

[18] F. Biscani, G. Giunta, S. Belouettar, E. Carrera, and H. Hu. Variable kinematic plate elements coupled via arlequin method. *International Journal for Numerical Methods in Engineering*, 91(12):1264–1290, 2012.

[19] E. Carrera, G. Giunta, and M. Petrolo. *Beam Structures: Classical and Advanced Theories.* John Wiley and Sons, 2011.

[20] E. Carrera and G. Giunta. Refined beam theories based on a unified formulation. *International Journal of Applied Mechanics*, 2(1):117–143, 2010.

[21] G. Giunta, G. De Pietro, H. Nasser, S. Belouettar, E. Carrera, and M. Petrolo. A thermal stress finite element analysis of beam structures by hierarchical modelling. *Composites Part B: Engineering*, 95:179–195, 2016.

[22] G. Giunta, N. Metla, S. Belouettar, A.J.M. Ferreira, and E. Carrera. A thermo-mechanical analysis of isotropic and composite beams via collocation with radial basis functions. *Journal of Thermal Stresses*, 36(11):1169–1199, 2013.

[23] E. Carrera, A. Garcia De Miguel, and A. Pagani. Hierarchical theories of structures based on Legendre polynomial expansions with finite element applications. *International Journal of Mechanical Sciences*, 120:286–300, 2017.

[24] E. Carrera, G. Giunta, P. Nali, and M. Petrolo. Refined beam elements with arbitrary cross-section geometries. *Computers & structures*, 88(5):283–293, 2010.

[25] A. Pagani, A. Garcia De Miguel, M. Petrolo, and E. Carrera. Analysis of laminated beams via unified formulation and Legendre polynomial expansions. *Composite Structures*, 156:78–92, 2016.

[26] K. J. Bathe. *Finite element procedures.* Prentice hall, 1996.

[27] E. Carrera, A. Garcia de Miguel, and A. Pagani. Extension of MITC to higher-order beam models and shear locking analysis for compact, thin-walled and composite structures. *International Journal for Numerical Methods in Engineering (In Press)*, 2017.

[28] K Washizu. Some considerations on a naturally curved and twisted slender beam. *Studies in Applied Mathematics*, 43(1-4):111–116, 1964.

[29] E. Carrera and G. Giunta. Hierarchical closed form solutions for plates bent by localized transverse loadings. *Journal of Zhejiang University SCIENCE A*, 8(7):1026 1037, 2007.

[30] E. Carrera and G. Giunta. Hierarchical models for failure analysis of plates bent by distributed and localized transverse loadings. *Journal of Zhejiang University SCIENCE A*, 9(5):600–613, 2008.

[31] A. G. de Miguel, G. De Pietro, E. Carrera, G. Giunta, and A. Pagani. Locking-free curved beam elements based on MITC for the analysis of composite laminates. *Manuscript submitted for publication.*

Tables

N	N_u	F_τ
0	1	$F_1 = 1$
1	3	$F_2 = \xi$ $F_3 = \eta$
2	6	$F_4 = \xi^2$ $F_5 = \xi\eta$ $F_6 = \eta^2$
3	10	$F_7 = \xi^3$ $F_8 = \xi^2\eta$ $F_9 = \xi\eta^2$ $F_{10} = \eta^3$
. . .	. . .	. . .
N	$\frac{(N+1)(N+2)}{2}$	$F_{\frac{(N^2+N+2)}{2}} = \xi^N$ $F_{\frac{(N^2+N+4)}{2}} = \xi^{N-1}\eta$ . . . $F_{\frac{N(N+3)}{2}} = \xi\eta^{N-1}$ $F_{\frac{(N+1)(N+2)}{2}} = \eta^N$

Table 1: Taylor's polynomials terms via Pascal's triangle.

	$10^9 \times u_\xi$	
Navier	8.0640	
N_e	B4	MITC4
60	8.0640	8.0640
40	8.0640	8.0640
20	8.0640	8.0640
10	8.0640	8.0640
8	8.0640	8.0640
6	8.0639	8.0640
4	8.0627	8.0640
2	7.9893	8.0619

Table 2: Transverse displacement u_ξ [m] for a very thick simply supported circular beam via TE2 model for different number of elements.

	u_ξ	
Navier	10.1613	
N_e	B4	MITC4
60	10.1613	10.1613
40	10.1613	10.1613
20	10.1587	10.1613
10	10.0565	10.1613
8	9.9082	10.1613
6	9.5641	10.1613
4	8.7190	10.1613
2	5.8122	10.1587

Table 3: Transverse displacement u_ξ [m] for a very slender simply supported circular beam via TE2 model for different number of elements.

	$10^7 \times u_s$		$10^7 \times u_\xi$	
PLANE183	3.0563		4.1860	
	FEM	Navier	FEM	Navier
TE5, HL5	3.0563	3.0563	4.1860	4.1860
TE4, HL4	3.0563	3.0563	4.1860	4.1860
TE3, HL3	3.0563	3.0563	4.1859	4.1859
TE2, HL2	3.0490	3.0490	4.1762	4.1762

Table 4: Displacement components [m] for a thick simply supported circular beam.

	Radial force F_ξ	Axial force F_s	Uniform pressure $p_\xi b$
	$10^6 \times \tilde{u}_\xi$	$10^6 \times \tilde{u}_s$	$10^5 \times \tilde{u}_\xi$
PLANE183	0.2456	0.1488	0.1183
Tufekci and Arpaci [3]	0.2205^a	0.1412^a	-
	0.2488^b	0.1537^b	-
Litewka and Rakowski [10]	0.2205^a	0.1412^a	0.1190^a
	0.2488^b	0.1537^b	0.1180^b
TE5	0.2458	0.1493	0.1183
TE4	0.2457	0.1492	0.1183
TE3	0.2448	0.1478	0.1183
TE2	0.2410	0.1457	0.1185

a: Axial deformation only. b: Axial and shear deformation.

Table 5: Dimensionless displacement components for a thick clamped-clamped circular beam via CUF TE-based 1D finite elements.

Figures
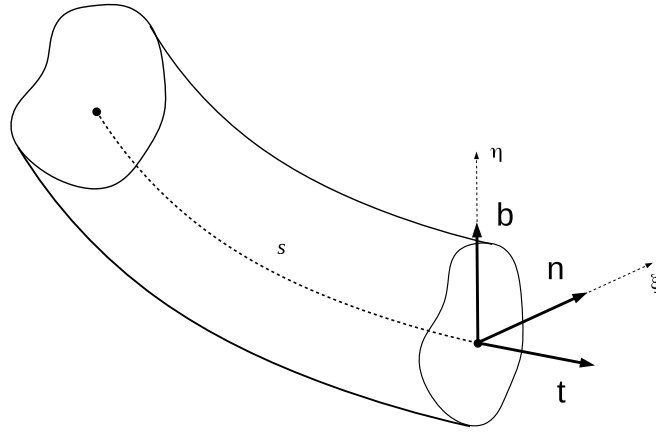
Figure 1: Curved beam structure and Frenet-Seret coordinate system.
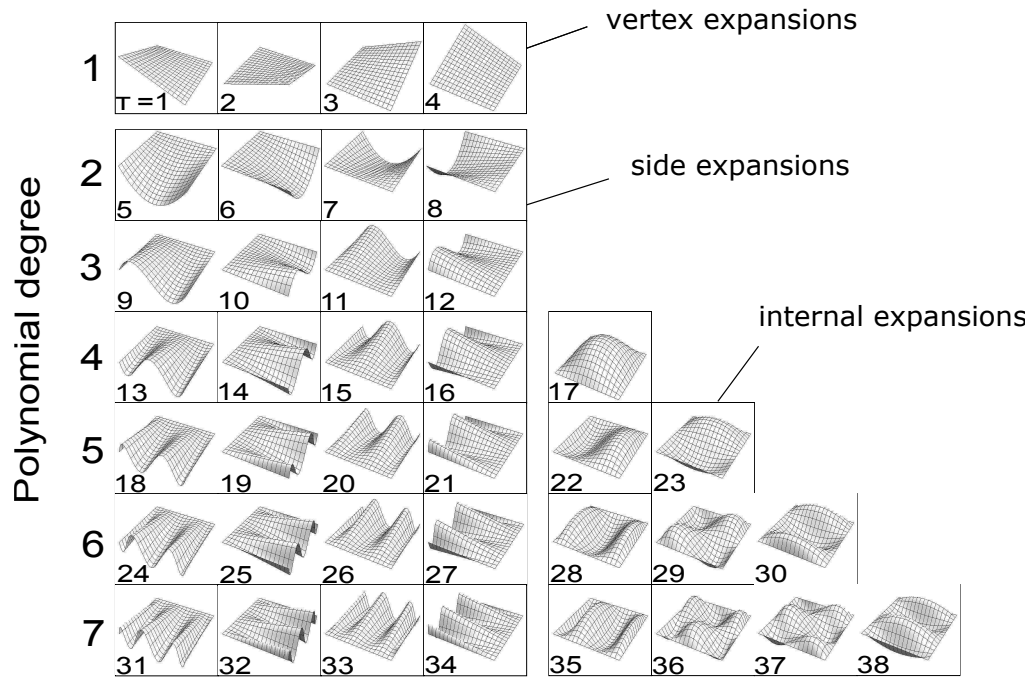
Figure 2: HLE set of expansion functions up to the order $p = 7$.
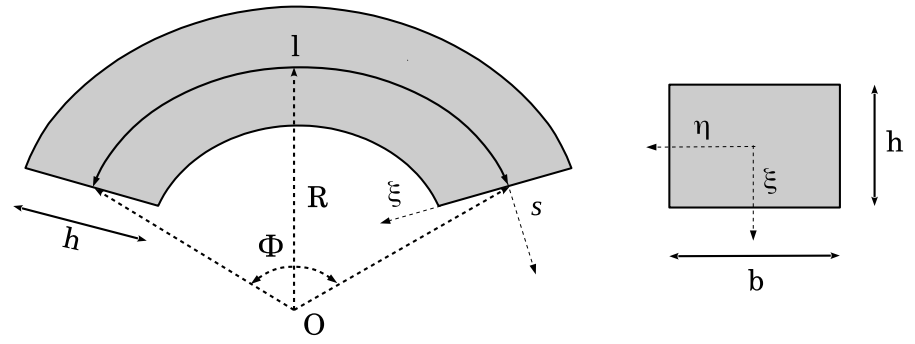
Figure 3: Geometry of a thick arch and cross-section.
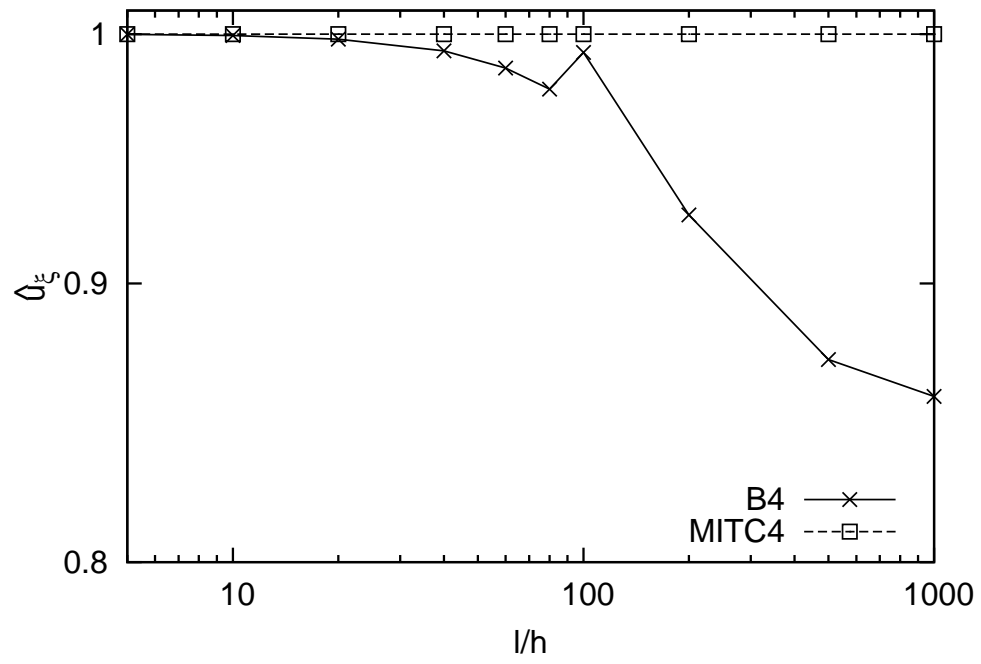
Figure 4: Shear locking correction via MITC for four-nodes elements, simply supported circular beam.
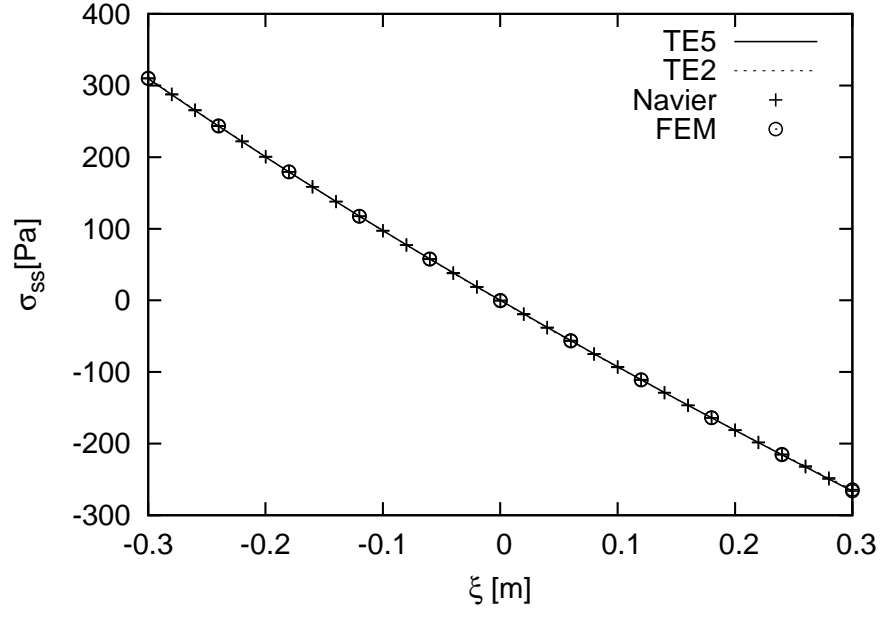
Figure 5: Axial stress σ_{ss} at $s = l/2$ for a thick simply supported circular beam obtained via FEM and Navier solution for different Taylor expansions.
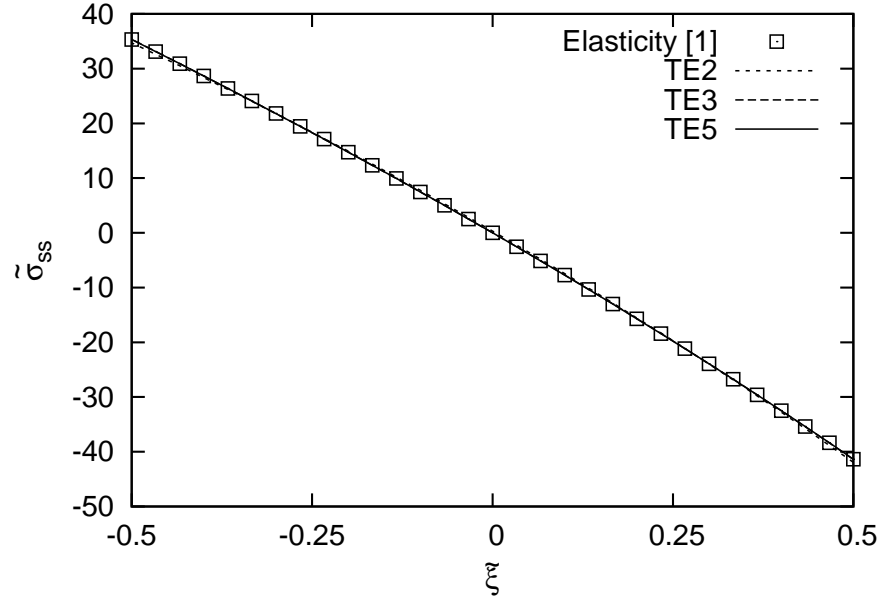
Figure 6: Radial stress $\sigma_{\xi\xi}$ at $s = l/2$ for a thick simply supported circular beam obtained via FEM and Navier solution for different Taylor expansions.
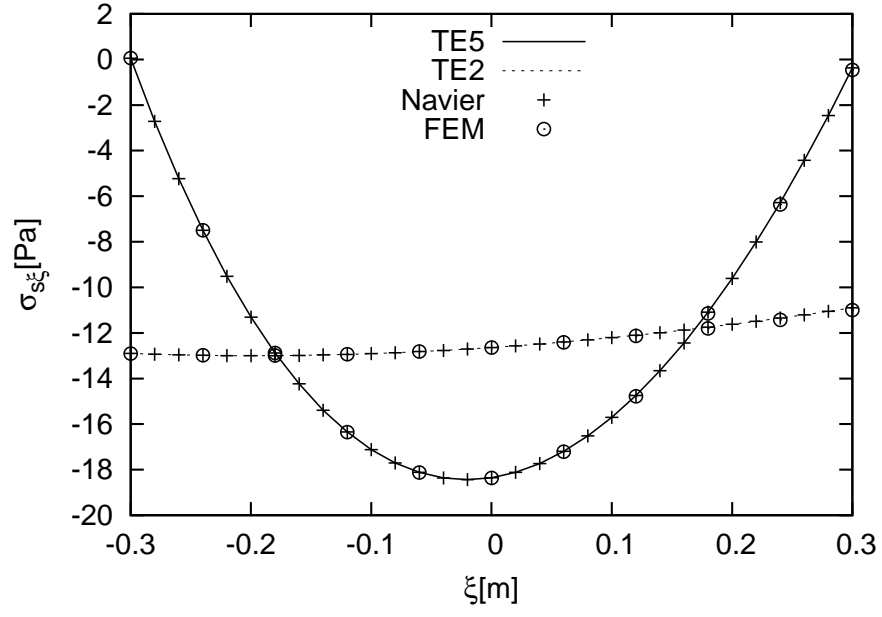
Figure 7: Shear stress $\sigma_{s\xi}$ at $s = 0$ for a thick simply supported circular beam obtained via FEM and Navier solution for different Taylor expansions.

Figure 8: Dimensionless axial stress $\tilde{\sigma}_{ss}$ at $s = l/2$ for a thick cantilever circular beam obtained by the proposed finite elements and an elasticity solution.
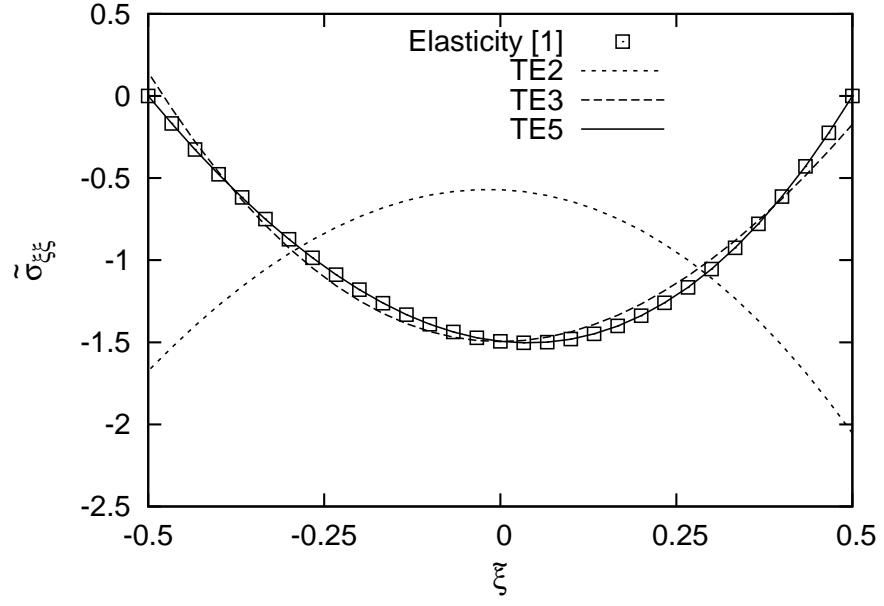
Figure 9: Dimensionless radial stress $\tilde{\sigma}_{\xi\xi}$ at $s = l/2$ for a thick cantilever circular beam obtained by the proposed finite elements and an elasticity solution.
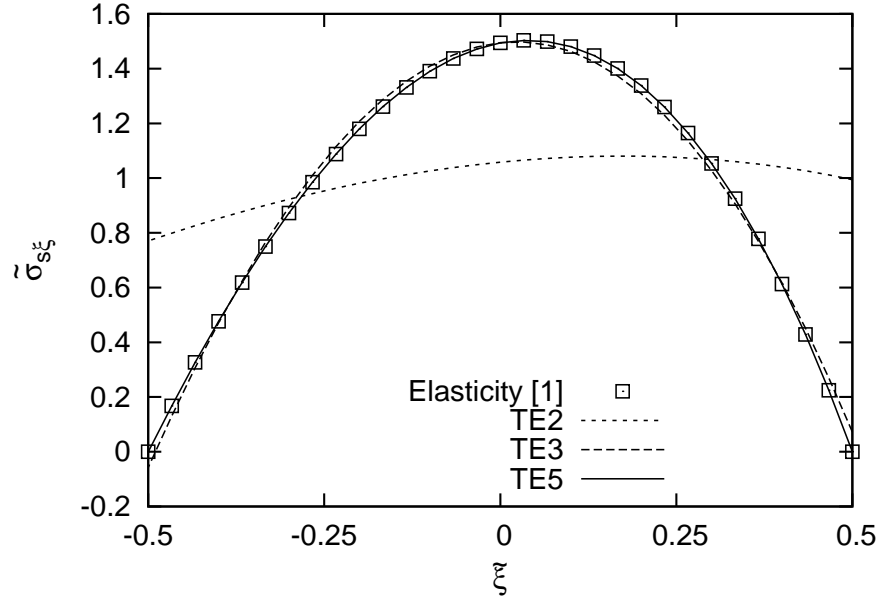
Figure 10: Dimensionless shear stress $\tilde{\sigma}_{s\xi}$ at $s = l/2$ for a thick cantilever circular beam obtained by the proposed finite elements and an elasticity solution.
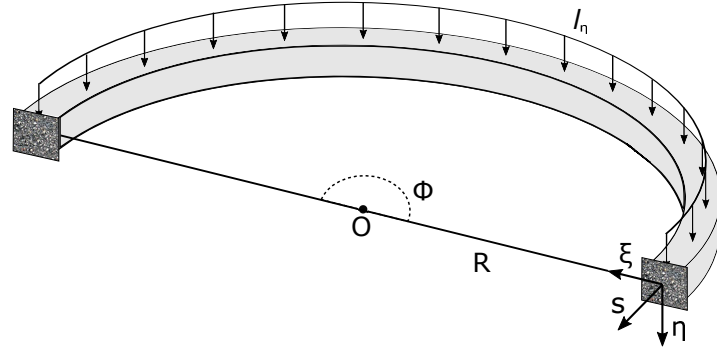
Figure 11: Geometry and loading of the 3D balcony problem.
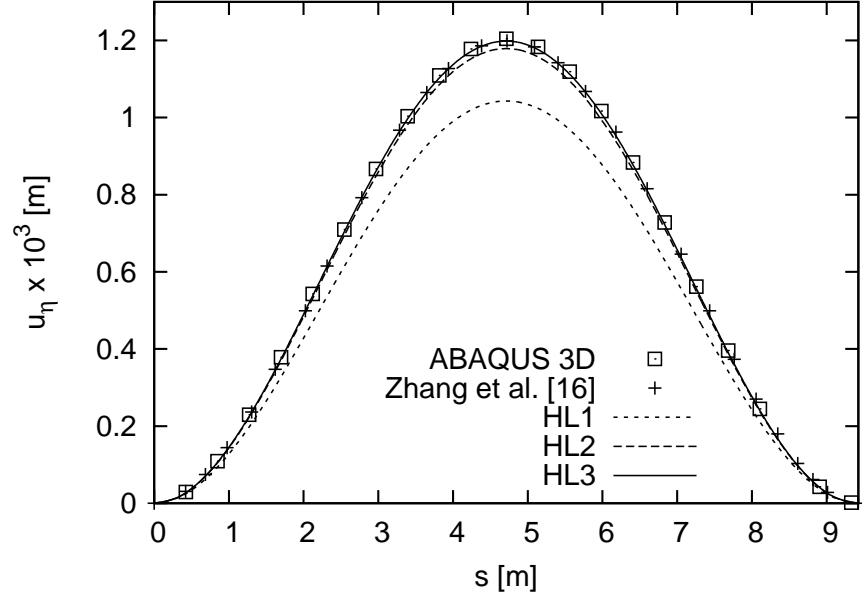
Figure 12: Transverse displacement u_η along the arc-length s for the balcony structure.
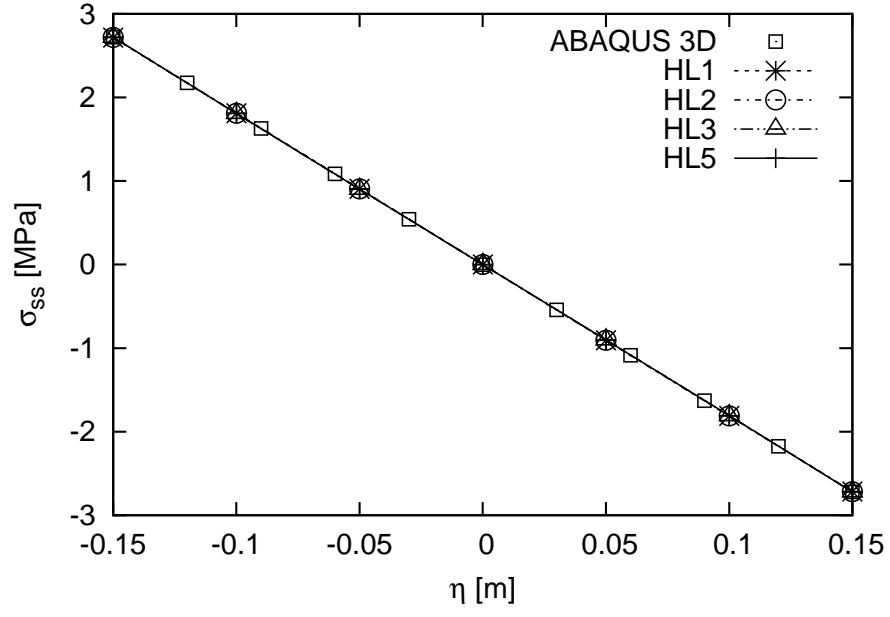
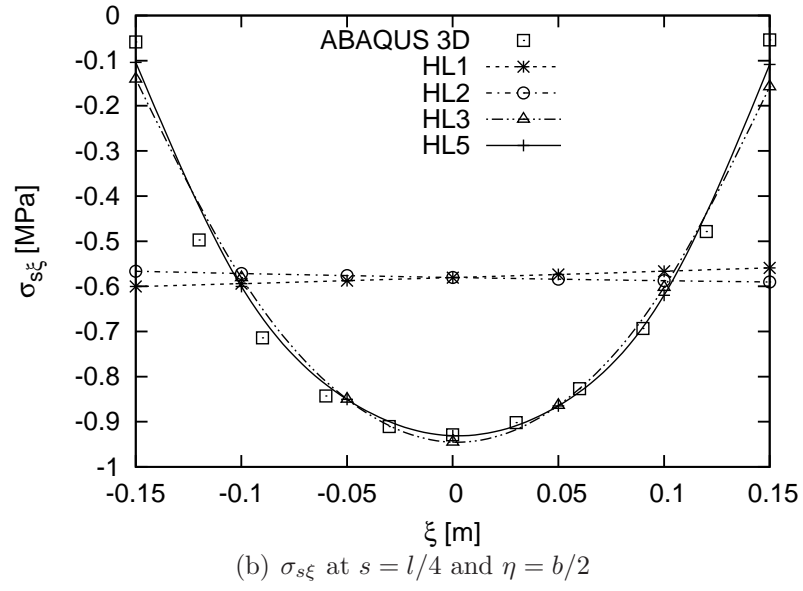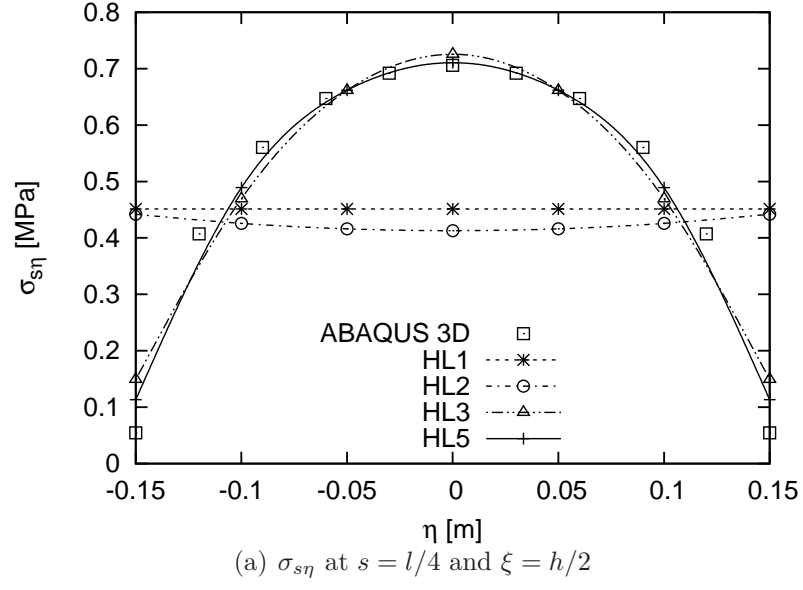Figure 13: Axial stress σ_{ss} at $s = l/2$ and $\xi = h/2$ for the balcony structure.

(a) $\sigma_{s\eta}$ at $s = l/4$ and $\xi = h/2$

(b) $\sigma_{s\xi}$ at $s = l/4$ and $\eta = b/2$

Figure 14: Transverse shear stresses for the balcony structure.

(a) 3D FEM

(b) CUF HL5
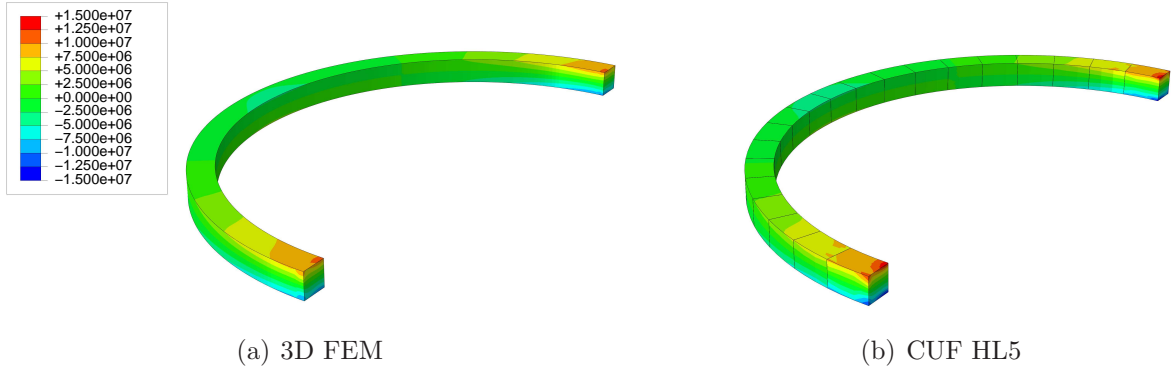
Figure 15: Three-dimensional distribution of the axial stress σ_{ss}.

(a) 3D FEM

(b) CUF HL5
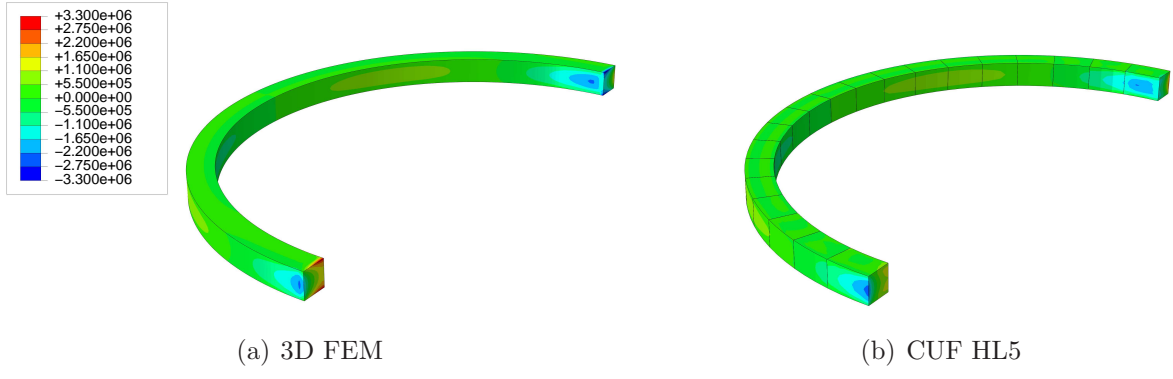
Figure 16: Three-dimensional distribution of the transverse shear stress $\sigma_{s\eta}$.
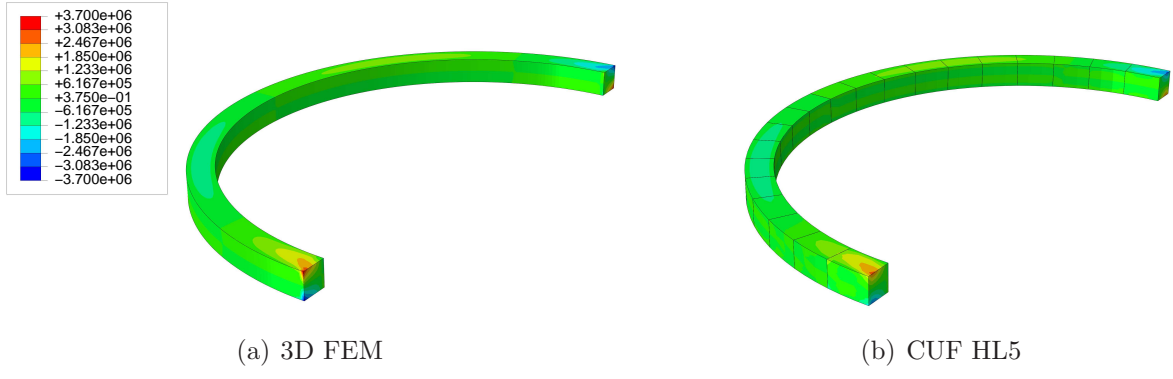
(a) 3D FEM   (b) CUF HL5

Figure 17: Three-dimensional distribution of the transverse shear stress $\sigma_{s\xi}$.